Ionics (2018) 24:1007–1017
DOI 10.1007/s11581-017-2255-y

ORIGINAL PAPER

Electrical, electrochemical, and cycling studies of high-power layered $Li(Li_{0.05}Ni_{0.7-x}Mn_{0.25}Co_x)O_2$ ($x = 0$, 0.1, 0.3, 0.5, and 0.7) cathode materials for rechargeable lithium ion batteries

A. Nichelson [1,2] · K. Karuppasamy [3] · S. Thanikaikarasan [1] · P. Anil Reddy [4] · Pratap Kollu [5,6] · S. Karthickprabhu [7] · X. Sahaya Shajan [1]

Received: 4 November 2016 / Accepted: 9 August 2017 / Published online: 29 August 2017

Abstract The enriched lithium ion containing layered oxide cathode materials $Li(Li_{0.05}Ni_{0.7-x}Mn_{0.25}Co_x)O_2$ have been prepared by using facile sol–gel technique. The phase purity and crystalline nature of the layered oxide cathodes have determined by X-ray diffraction analysis. Surface morphology and elemental analysis have been carried out using scanning electron microscopy with energy dispersive analysis by X-rays and HR-TEM. Cyclic voltammetry analysis of the lithium-enriched cathode material shows a well redox performance at electrode–electrolytic interface. The $Li(Li_{0.05}Ni_{0.7-x}Mn_{0.25}Co_x)O_2$ cathode shows the most promising electrochemical properties under different conditions in which an appropriate rising of discharge capacity (i.e., 167 mAh g^{-1} at 0.5 C) and cycling stability (i.e., capacity retention: 83% at 1 C after 20 cycles, cutoff voltage 2.8–4.5 V) at ambient temperature. These unique properties allow the effective use of these cathode materials as positive electrodes for the development of rechargeable lithium ion batteries.

Keywords Sol–gel technique · Nanomaterials · Li-ion batteries · Cyclic voltammetry

Pratap Kollu: Newton Alumnus Researcher.

✉ X. Sahaya Shajan
shajan89@gmail.com

1 Centre for Scientific and Applied Research, PSN College of Engineering and Technology, Tirunelveli, Tamilnadu 627152, India

2 St. Mother Theresa Engineering College, Vagaikulam, Mudivaithanenthal Post, Thoothukudi, Tamil Nadu 628 102, India

3 Division of Electronics and Electrical Engineering, Dongguk University-Seoul, Seoul 04620, South Korea

4 Department of Metallurgical Engineering and Materials Science, Indian Institute of Technology Bombay, Powai, Mumbai 400076, India

5 CASEST, School of Physics, University of Hyderabad, Gachibowli, Hyderabad 500046, India

6 Department of Physics, Cavendish Laboratory, University of Cambridge, Cambridge CB3 0HE, UK

7 K.Ramakrishnan College of Technology, Samayapuram, Trichy, Tamil Nadu 621112, India

Introduction

Recent years, lithium ion batteries (LIBs) are gaining a great deal of attention in portable electric devices including cellular phones, digital cameras, and laptops due to their admirable properties like high specific energy, high adoptability, and slow loss of charge, etc., The common drawback that we come across is their high cost, power, and cycle life. In the past two decades, a numerous number of layered oxide materials (LOM) were employed as cathodes in LIBs and they show promising improvement on conductivity and cycling point of view compared to conventional cathodes [1]. In the first generation, layered lithium cobalt oxide ($LiCoO_2$) cathode material exhibits a theoretical capacity value of around 272 mAh g^{-1} [2]. But in practical, it delivers only half of its theoretical capacity (140 mAh g^{-1}) in practical cells. This may possibly be due to its extraction of half quantity of lithium from $LiCoO_2$ in the form of $Li_{0.5}CoO_2$ [3]. Hence, researchers and scientific communities have been focused towards the direction of fabricating cost-effective and ecofriendly high-capacity cathodes using substituted layered oxide materials [4–8]. Some of the niceties of LOMs were reported elsewhere [9]. To explain in brief, the substitution of cobalt (Co) with nickel (Ni) and manganese (Mn) oxides improves the structural stability upon its cycling [10, 11]. The effect of ruthenium substitution for Mn in $Li_{1.2}Mn_{0.567}Ni_{0.166}Co_{0.067}O_2$ Li-rich material has been investigated by Haijun Yu and Haoshen Zhou and achieved a discharge capacity of 284 mAh g^{-1} [12]. Further, the increase in

the value of coulombic efficiency may be attributed to the decrease in the value of the ratio between initial irreversible capacity and initial charge capacity, associated with the decrease in the value of the content of Li_2MnO_3 component or Li_2MnO_3 component which can be activated inside these materials. Yukinori Koyama et al. have been proposed theoretical models about $[Co_{1/3}Ni_{1/3}Mn_{1/3}]O_2$ ($0 \le x \le 1$) compound and investigated density of states and electronic structures of the proposed models [13]. Liu and his coworkers have been investigating the effect of dopants Co, Mn, and Mg on lithium nickel oxides and indicated that the substitution of Mn, Mg suppresses the impedance of the cell rather than the substitution of Co [14, 15]. In the recent years, researchers have been focused to obtain a better composition in $LiNiMnCoO_2$ cathode systems in order to overcome the constraints of cathodes; mostly, they raised charge–discharge rates at higher temperature. Several methods have been employed to prepare the $LiNiMnCoO_2$ system with outstanding properties which include sol–gel process, coprecipitation [16–18], combustion [19], solid-state reaction [20–22], and spray pyrolysis techniques [23]. Among, the preparation of cathode materials by the sol–gel technique has been served as a promising candidate [24] due to its excellent particle size with better stoichiometry.

In the present work, the cathode material lithium-rich $Li(Li_{0.05}Ni_{0.7-x}Mn_{0.25}Co_x)O_2$ with x values in the range between 0 and 0.7 has been prepared for the first time by citric acid-assisted modified sol–gel technique. Here, citric acid acts as chelating agent, showed the way to decompose nitrate ions, and evolutes ion in the form of heat which has been utilized to ignite the remaining organic constituents [25]. The effect of Co and Ni composition on structural, morphological, elemental, optical, and electrochemical properties has been investigated thoroughly. Moreover, cathode materials considered in the present study can be synthesized with typical rhombohedral structure and can show monotonous charge–discharge behavior. Even though lot of articles were published in this sense, this article entirely spotlights on the importance of lithium-rich layered $Li(Li_{0.05}Ni_{0.7-x}Mn_{0.25}Co_x)O_2$ for battery applications and has been studied for the first time. The details are presented herein.

Experimental

Synthesis of $Li(Li_{0.05}Ni_{0.7-x}Mn_{0.25}Co_x)O_2$ compounds

All the precursor materials used in the present work were analytical grade reagents (Merck). Lithium nitrate ($LiNO_3$), manganese nitrate [$Mn(NO_3)_2{\cdot}6H_2O$], nickel nitrate [$Ni(NO_3)_2{\cdot}6H_2O$], and cobalt nitrate [$Co(NO_3)_2{\cdot}6H_2O$] were served as starting materials and used without further purifications. Citric acid ($C_6H_8O_7$) was obliged as a chelating agent. In the whole synthesis process, double deionized water having a conductivity of 18 Ω cm^{-2} was used as a solvent. Before used for preparation, the compounds were dried in vacuum at a temperature of around 50 °C. Thereafter, dried compounds were dissolved in deionized water and the solution was stirred slowly for the time duration of 7 h with the help of magnetic stirrer cum heater at a temperature of 70 °C. During the initial stage, the pH of the homogeneous solution was maintained at 5.5 ± 0.5. In order to reduce the pH of the solution into 2.0 ± 0.5, citric acid was added dropwise into the reaction mixture. Further, the inclusion of liquid ammonia led to increase the value of pH 7.0 ± 0.5. Finally, the ammoniated reaction mixture was heated to 80 °C with constant stirring that leads to the formation of gel. The obtained gel was transferred to alumina crucible and preheated to 500 °C for the time duration of 4 h. Finally, we were obtained sample in the form of powder. Thereafter, the powder sample was grinded well for the time duration of 2 h and then heated to 850 °C for 15 h. The obtained powder samples were kept inside a glove box in order to avoid moisture effects and contamination.

Characterization

The X-ray diffraction data of the prepared samples was recorded using an (XPERT-PRO PANalytical, Netherlands) X-ray diffractometer with CuKα radiation (λ = 1.5418 Å). Surface morphology and elemental composition were analyzed using an energy-dispersive analysis by X-ray set up attached with scanning electron microscope (JEOL JSM-6400, Japan). The TEM image analysis was done using the transmission electron microscope (PHILIPS CM 200). Fourier transform infrared spectroscopic analysis was carried out using an FTIR spectrometer (JASCO 4100, Japan) within the wave number range between 400 and 4000 cm^{-1}. Electrochemical impedance spectroscopic analysis was carried out using an electrochemical workstation (Zahner IM6, Germany). Cyclic voltammetry as well as charge–discharge characteristics of the fabricated coin cells were analyzed using potentiostat/galvanostat (SP-300 BioLogic, France).

Fabrication of electrodes and cell assembly

The positive electrodes were prepared using 80 wt% of $Li(Li_{0.05}Ni_{0.4}Mn_{0.25}Co_{0.3})O_2$, 10 wt% of carbon black, and 10 wt% polyvinylidene fluoride (PVDF). The average loading density of active material was 2.904 mg. The active material was laminated on aluminum foil as cathode, lithium metal as anode, respectively. Also, lithium hexafluorophosphate ($LiPF_6$) was dissolved in a mixture of ethylene carbonate (EC) and dimethyl carbonate (DMC) in the volumetric ratio (1:1) as an electrolyte and porous polypropylene membrane (Celgard 2400) as a separator between cathode and anode, respectively. The fabrication of coin cells was carried out using the abovementioned components as cathode, anode,

electrolyte, and separator with the help of an argon-filled glove box (Mikrouna, China). The fabricated coin cells were subjected to cyclic voltammetry, electrochemical impedance spectroscopy, and charge–discharge characteristics using SP-300 (BioLogic, France) potentiostat/galvanostat.

Results and discussion

X-ray diffraction analysis

The X-ray diffraction (XRD) pattern of $Li(Li_{0.05}Ni_{0.7-x}Mn_{0.25}Co_x)O_2$ compound with various "x" values in the range between 0.1 and 0.7 is shown in Fig. 1. As it can be seen, the 2θ values at 38°, 65° correspond to the lattice planes (0 0 6/0 1 2), (0 1 8/1 1 0), respectively. The value of the interplanar spacing "d" is calculated by means of using Eq. (1) [26, 27]. The d values observed in the present work are compared with standard file values (JCPDS no. 44-0145) which resemble a hexagonal α–$NaFeO_2$ structure with the space group $R\bar{3}$ m (166) [28–30]. The presence of alternate layers such as the Li atom and the molecule MO_6 (M = Ni, Co, Mn) in an octahedral form

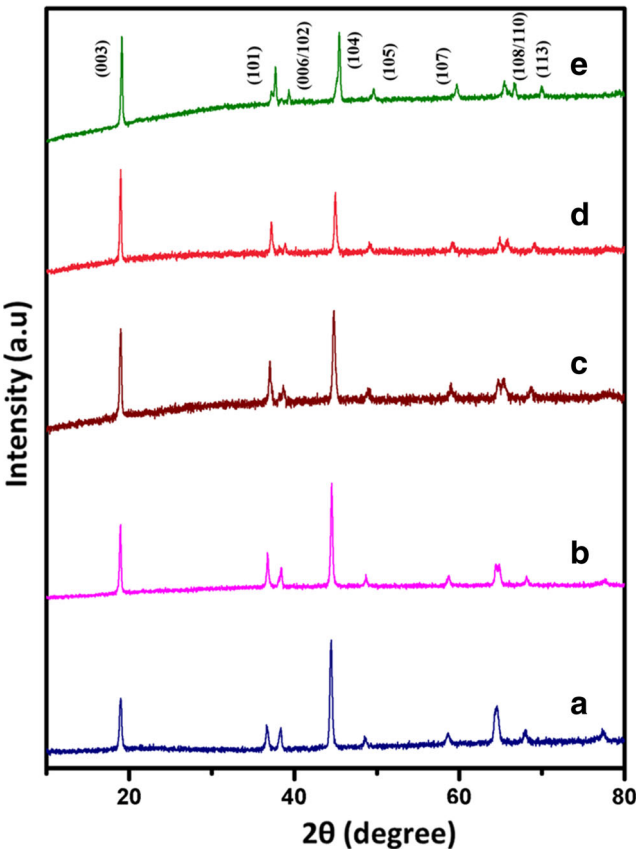

Fig. 1 X-ray diffraction pattern of $Li(Li_{0.05}Ni_{0.7-x}Mn_{0.25}Co_x)O_2$ compound obtained at various compositional values: (a) x = 0, (b) x = 0.1, (c) x = 0.3, (d) x = 0.5, and (e) x = 0.7

indicates that the layered crystal structure is in pure form [31]. Also, it seems that the peaks at 38 and 65° correspond to a well-grown layered structure. At lower values of x, it is denoted that the peaks corresponding to the lattice planes (0 0 6/1 0 2) and (0 1 8/1 1 0) are merged together to form a single peak that resembles the complete cubic structure [32]. The formation of an ideal layered structure can be observed for the higher values of composition x. A similar formation of a layered structure with the molecular formula $LiNi_{1/3}Mn_{1/3}Co_{1/3}O_2$ has been reported earlier by Kim et al. [33]. The intensity ratio of the peaks with lattice planes I_{003} and I_{104} gives the information about cationic mixing in the cathode material. The critical value of the I_{003}/I_{104} ratio is 1.2 for the layer structured material [34]. When it is less than the critical value, there is a significant amount of cationic mixing and the cationic mixing is absent for the values greater than the critical value. The ratio of I_{003}/I_{104} is found to be increased from 0.94 to 1.25 as the cobalt content increases from 0 to 0.7.

$$2d\sin\theta = n\lambda \tag{1}$$

$d_{hkl} = \frac{\lambda}{2sin\theta}$ where d is the interplanar spacing, θ is the diffraction angle, n is the order of diffraction, and λ is wavelength of X-rays used. The observed value of lattice parameters "a" and "c" are calculated using Eq. (2) [35].

$$\frac{1}{d^2} = \frac{4}{3}\left[\frac{h^2 + hk + k^2}{a}\right] + \left[\frac{l^2}{c^2}\right] \tag{2}$$

The unit cell is the parallelepiped built on the vectors a, b, c, of a crystallographic basis of the direct lattice. The unit cell volume is given by the scalar triple product, $V = (a, b, c)$, which corresponds to the square root of determinant of the metric tensor. The total volume of the unit cell (V) is calculated using Eq. (3) [36].

$$V = \frac{\sqrt{3}a^2c}{2} \tag{3}$$

Variation of lattice constant a with composition x values for $Li(Li_{0.05}Ni_{0.7-x}Mn_{0.25}Co_x)O_2$ compound obtained at various Ni and Co concentrations is shown in Fig. 2a. It is observed in Fig. 2a that the value of a is found to decrease, if the value of x is increased from 0 to 0.1. Thereafter, above 0.1, there is slight decrement is observed which is denoted in the figure. Figure 2b shows the variation of c with various x values for $Li(Li_{0.05}Ni_{0.7-x}Mn_{0.25}Co_x)O_2$ compound obtained at various Ni and Co concentrations. It is noted that the value of c is found to decrease, whereas the value of x increases, except the

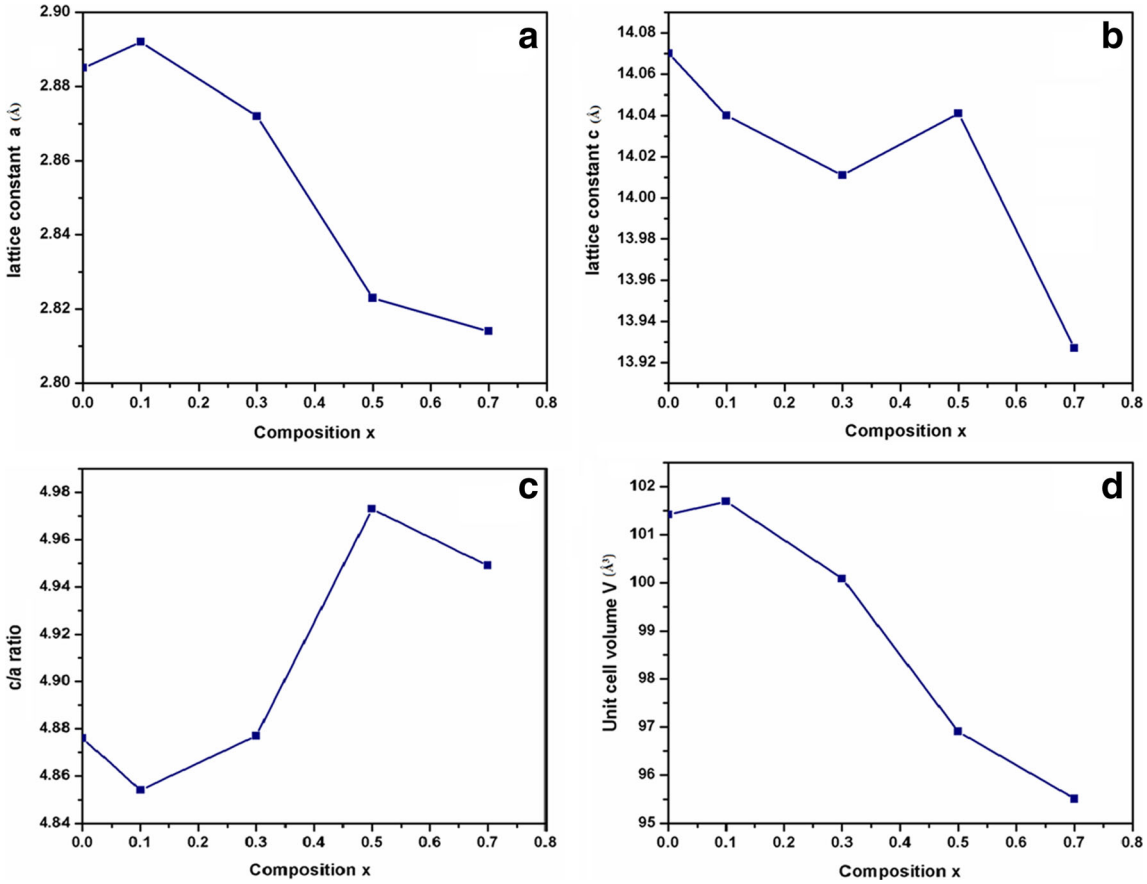

Fig. 2 **a** Variation of lattice constant "*a*" with respect to "*x*" of compound $Li(Li_{0.05}Ni_{0.7-x}Mn_{0.25}Co_x)O_2$ obtained at different conditions: (a) $x = 0$, (b) $x = 0.1$, (c) $x = 0.3$, (d) $x = 0.5$, and (e) $x = 0.7$. **b** Variation of lattice constant "*c*" with respect to *x* of compound $Li(Li_{0.05}Ni_{0.7-x}Mn_{0.25}Co_x)O_2$ obtained at different conditions: (a) $x = 0$, (b) $x = 0.1$, (c) $x = 0.3$, (d) $x = 0.5$, and (e) $x = 0.7$. **c** Variation of the "*c*/*a*" ratio with respect to *x* of compound $Li(Li_{0.05}Ni_{0.7-x}Mn_{0.25}Co_x)O_2$ obtained at different conditions: (a) $x = 0$, (b) $x = 0.1$, (c) $x = 0.3$, (d) $x = 0.5$, and (e) $x = 0.7$. **d** Variation of unit cell volume "*V*" with respect to *x* of compound $Li(Li_{0.05}Ni_{0.7-x}Mn_{0.25}Co_x)O_2$ obtained at different conditions: (a) $x = 0$, (b) $x = 0.1$, (c) $x = 0.3$, (d) $x = 0.5$, and (e) $x = 0.7$

value of $x = 0.5$. Variations observed in a and c values lead to produce similar variation in the c/a ratio and unit cell volume which is shown in Fig. 2c, d. It is noted that there is there is a gradual decrease in the unit cell volume with respect to the concentration of Co and Ni in the prepared samples which may be due to the value of ionic radius of Co^{3+} (0.545 Å) which is smaller than Ni^{2+} (0.69 Å). The sizes of the crystallites formed in the prepared samples are calculated using the FWHM data and Debye–Scherrer's formula [35]

$$D = \frac{0.9\lambda}{\beta\cos\theta} \tag{4}$$

where λ is the wavelength of X-rays used ($\lambda = 1.5406$ Å), β is the full width at half-maximum of the peak position in radian, and θ is the Bragg's diffraction angle at the peak position in degrees. The sizes of the crystallites obtained in the present work are in the range between 60 and 80 nm.

Vibrational spectroscopic analyses

FTIR spectra recorded for $Li(Li_{0.05}Ni_{0.7-x}Mn_{0.25}Co_x)O_2$ samples prepared at various *x* values are shown in Fig. 3i. The peaks that appeared at 570, 576, 591, 606, and 609 cm^{-1} correspond to asymmetric stretching mode of M–O (M = Ni, Co, Mn) in the compounds, respectively. Moreover, the appearance of the peak at 530 cm^{-1} may be assumed to represent stretching vibration of Li–O which is confirmed by the presence of elements in the prepared samples and the results reported elsewhere, also, a peak at 271 cm^{-1} is expected [19, 37]. The O–M–O bending mode in lithium-enriched $Li(Li_{0.05}Ni_{0.7-x}Mn_{0.25}Co_x)O_2$ is confirmed by the identification of peak at 419, 420, 425, 426, and 431 cm^{-1}, respectively. The obtained results resemble with the result reported earlier by Julien et al. [38]. The observed findings clearly conclude that there is a strong interaction between metal and oxygen in the formation of compound obtained at various *x* values. The observed results are further confirmed by Raman analysis which will be discussed later in the following sections.

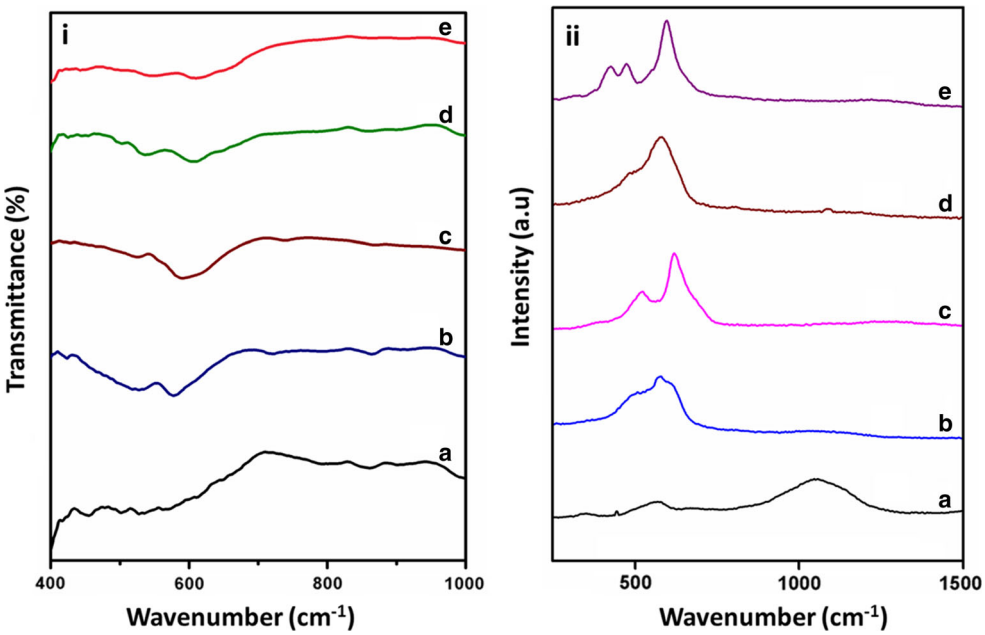

Fig. 3 **i** FTIR spectra recorded for $Li(Li_{0.05}Ni_{0.7-x}Mn_{0.25}Co_x)O_2$ compound obtained at various compositional values: (a) $x = 0$, (b) $x = 0.1$, (c) $x = 0.3$, (d) $x = 0.5$, and (e) $x = 0.7$. **ii** Raman spectra recorded for $Li(Li_{0.05}Ni_{0.7-x}Mn_{0.25}Co_x)O_2$ compound obtained at various compositional values (a) $x = 0$, (b) $x = 0.1$, (c) $x = 0.3$, (d) $x = 0.5$, and (e) $x = 0.7$

In order to validate the FTIR results and to identify the various possible interactions of ions in the prepared cathode materials, we have performed Raman analysis using Renishaw inVia Raman spectrophotometer. Raman spectra recorded $Li(Li_{0.05}Ni_{0.7-x}Mn_{0.25}Co_x)O_2$ samples prepared at various x values are shown in Fig. 3ii. It is quite observed from the spectra that the peaks at 571 and 476 cm^{-1} correspond to metal oxide symmetric stretching and bending modes, respectively. For the layered structure cathodic material with a space group $R\bar{3}$ m (166) which is similar to the compound $LiCoO_2$, the corresponding optical vibrations are $\Gamma = A_{2g} + E_g + 2A_{2u} + 2E_u$ [37]. The first two modes are visible in Raman while the second two modes can be visible by IR. Theoretically, two Raman bands and four IR bands should be visible for the layer structured material with the space group $R\bar{3}$ m [39]. Figure 3ii (b–e) shows the peaks around 571 and 476 cm^{-1} which may correspond to active M–O symmetric stretching and bending, vibrational, Raman modes of A_{1g} and E_g. The appearance of a hump along with these modes appeared in Fig. 3ii (e) corresponding to the higher value of x. The additional peaks observed in Fig. 3ii (a) show the cubical phase which reflects the observation made in XRD [40].

Morphological analyses

Scanning electron microscopic images of $Li(Li_{0.05}Ni_{0.7-x}Mn_{0.25}Co_x)O_2$ samples prepared at various x values are shown in Fig. 4a–e. As it can be seen, the SEM images of prepared cathode materials consist of spherical shaped nanoparticles having the lateral dimensions ranging from 200 to 250 nm as shown in Fig. 4. The bigger particle size may be due to evenly distributed crystallites leads to form the agglomerated spherical shaped particles (formed during loading of samples) as indicated in Fig. 4. The sizes of the particles are found to be in the range between 200 and 250 nm which in turn supports the results obtained by powder XRD analysis as discussed earlier (calculated crystallite size is in the range between 60 and 80 nm). The decrease in value of particle size may be due to the addition of citric acid as a chelating agent with a precursor followed by the process of calcination. Hence, the surface area of the prepared samples was found to be large which can shorten the diffusion path of lithium ions that helped to improve the electrochemical performance of the prepared cathodic material. The observed results are in concordance with the result reported earlier by Jin et al. [41].

In order to validate SEM results as well as to know the particle size, HR-TEM analysis has been performed. Figure 5a, b represents the TEM images of $Li(Li_{0.05}Ni_{0.4}Mn_{0.25}Co_{0.3})O_2$ sample. It is observed that the particles are in the cylindrical polyhedron shape and having the diameter of a sphere was estimated to be 200–250 nm, which is in agreement with the SEM image results. Also, the particle size is observed to be around 250 nm which in turn confirms the good crystallinity of the particles. The current finding strongly strengthens the result obtained by SEM analysis and is in concurrent with the results reported earlier by Ghosh et al. [42].

The EDX spectra of $Li(Li_{0.05}Ni_{0.7-x}Mn_{0.25}Co_x)O_2$ samples obtained at various x values are shown in Fig. 6i. The presence of emission lines in the investigated energy range indicates the formation of $Li(Li_{0.05}Ni_{0.7-x}Mn_{0.25}Co_x)O_2$. The emission lines of the lithium element are not found in the EDX spectra which must be due to lower value of its atomic number [41].

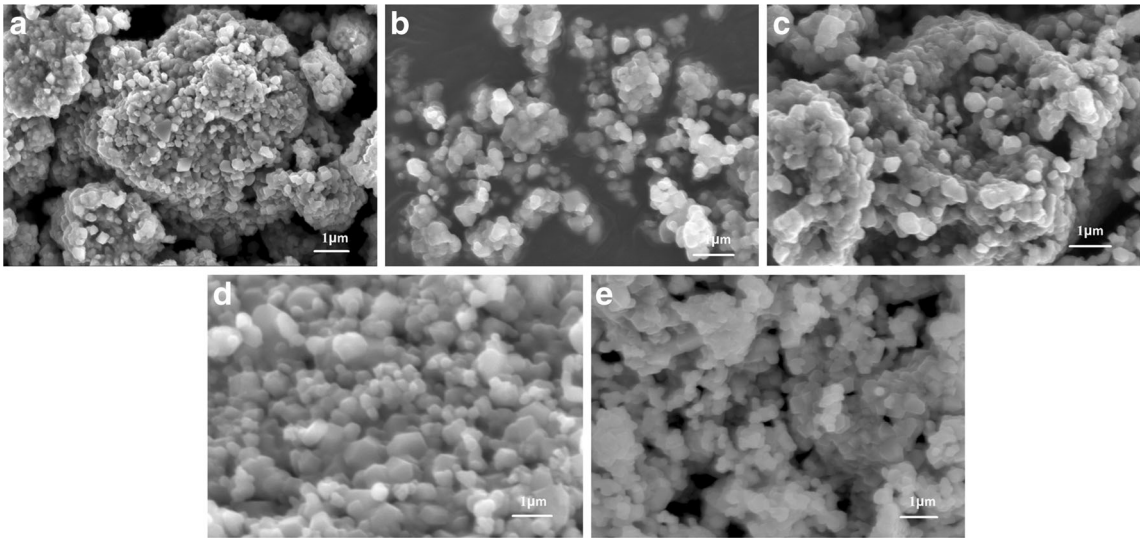

Fig. 4 Scanning electron microscopic images for $Li(Li_{0.05}Ni_{0.7-x}Mn_{0.25}Co_x)O_2$ compound obtained at various compositional values. **a** $x = 0$. **b** $x = 0.1$. **c** $x = 0.3$. **d** $x = 0.5$. **e** $x = 0.7$

But in the meantime, the presence of lithium in the prepared sample $Li(Li_{0.05}Ni_{0.4}Mn_{0.25}Co_{0.3})O_2$ has been confirmed by ^{7}Li-NMR as shown in Fig. 6ii. Hence to conclude, the prepared cathode materials consist of all the elements mentioned and are in resemblance with earlier reported results [43, 44]

Electrical analysis

The Nyquist impedance plot of the prepared $Li(Li_{0.05}Ni_{0.7-x}Mn_{0.25}Co_x)O_2$ with five different concentrations at ambient temperature is displayed in Fig. 7a. It reveals from the figure that all the five prepared samples exhibit a flattened semicircle (at high frequency) along with spiky lines at low frequencies. The flattened semicircle should comprise of a charge transfer resistance (interfacial resistance, R_{ct}) and a constant phase element (CPE) models, the behavior of a double layer in a non-ideal capacitor, while a small inclined spiky straight line at low frequency is related to the electrode polarization process. The bulk resistance is determined by means of intersecting with real axis Z', and its corresponding ionic conductivity has been evaluated by following expression:

$$\sigma = {}^{t}/_{AR_b} \tag{1}$$

Where R_b indicates bulk resistance and A and t signify the geometric area (πr^2) and thickness of the electrolyte–electrode interface. Figure 7b shows the ionic conductivity as a function of frequency for different ratios of cathode materials. It is to be noticed that among the prepared ratios, the sample with mole percentage $X = 3$, i.e., $Li(Li_{0.05}Ni_{0.7-x}Mn_{0.25}Co_x)O_2$, provides better room temperature ionic conductivity than that of other prepared samples. Hence, we focus our analysis towards the direction to measure the EIS of $Li(Li_{0.05}Ni_{0.7-x}Mn_{0.25}Co_x)O_2$ at different temperatures.

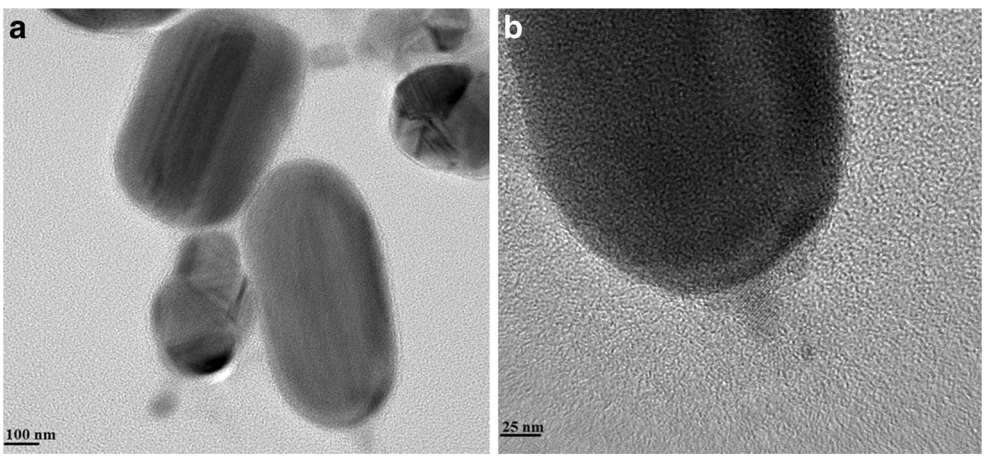

Fig. 5 **a**, **b** TEM micrographs of $Li(Li_{0.05}Ni_{0.4}Mn_{0.25}Co_{0.3})O_2$ prepared by sol–gel method

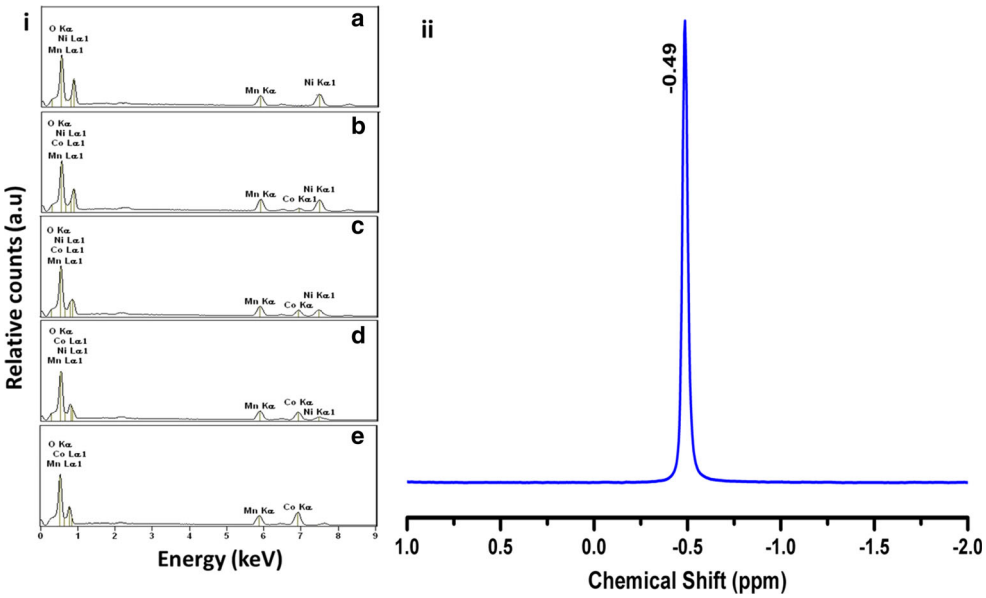

Fig. 6 **i** Energy-dispersive spectra for $Li(Li_{0.05}Ni_{0.7-x}Mn_{0.25}Co_x)O_2$ compound obtained at various compositional values: (a) $x = 0$, (b) $x = 0.1$, (c) $x = 0.3$, (d) $x = 0.5$, and (e) $x = 0.7$. **ii** ^{7}Li-NMR of $Li(Li_{0.05}Ni_{0.4}Mn_{0.25}Co_{0.3})O_2$

The ionic conductivity as a function of temperature for $Li(Li_{0.05}Ni_{0.4}Co_{0.3}Mn_{0.25})O_2$ has been measured by the way of subjecting $Li(Li_{0.05}Ni_{0.4}Mn_{0.25}Co_{0.3})O_2$/1 M $LiPF_6$/Li coin cell to EIS analysis at different temperatures in the range between 303 and 403 K. Figure 7c represents the conductance spectra and Nyquist impedance plot at different temperatures for $Li(Li_{0.05}Ni_{0.4}Co_{0.3}Mn_{0.25})O_2$. Its corresponding temperature dependence curve is shown in Fig. 7d. As it can be seen, the ionic conductivity increases with increase in temperature. The ionic conductivity of $Li(Li_{0.05}Ni_{0.4}Co_{0.3}Mn_{0.25})O_2$ obeys the Arrhenius law of conduction mechanism.

$$\sigma = \sigma_0 e^{-E_a/RT}$$

It is found that the samples exhibited an ionic conductivity value in the range between 10^{-5} and 10^{-4} S cm^{-1}. Its

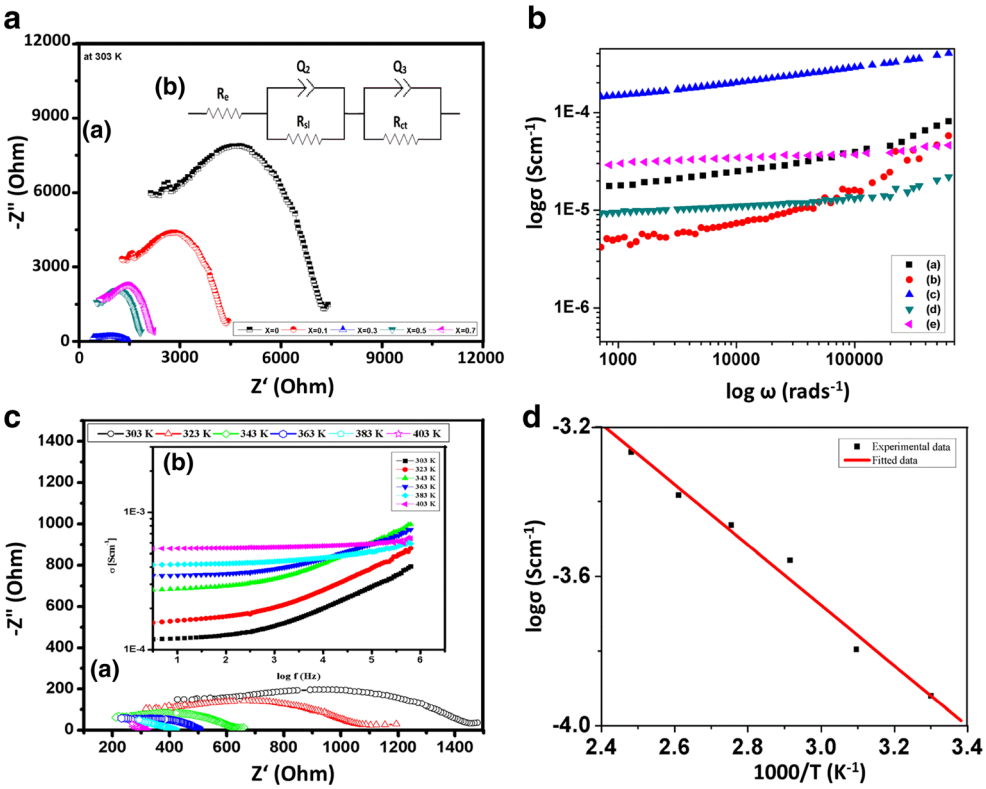

Fig. 7 **a** Nyquist impedance plot of $Li(Li_{0.05}Ni_{0.7-x}Mn_{0.25}Co_x)O_2$ compound obtained at various compositional values: (a) $x = 0$, (b) $x = 0.1$, (c) $x = 0.3$, (d) $x = 0.5$, and (e) $x = 0.7$ at ambient temperature (b) conductance spectra of $Li(Li_{0.05}Ni_{0.7-x}Mn_{0.25}Co_x)O_2$ compound obtained at various compositional values. **b** (a) $x = 0$, (b) $x = 0.1$, (c) $x = 0.3$, (d) $x = 0.5$, and (e) $x = 0.7$ at room temperature. **c** Nyquist impedance and conductance plot of $Li(Li_{0.05}Ni_{0.4}Mn_{0.25}Co_3)O_2$ at different temperatures. **d** log σ as a function of T for $Li(Li_{0.05}Ni_{0.4}Mn_{0.25}Co_{0.3})O_2$

corresponding equivalent circuit is represented in the inset in Fig. 2. The higher value of ionic conductivity of $Li(Li_{0.05}Ni_{0.4}Mn_{0.25}Co_{0.3})O_2$ at different temperature may be due to electrode polarization process. The obtained results are in concurrent with the earlier reported results [45, 46]

Cyclic voltammetric analysis

To perceive the electrochemical behavior of $Li(Li_{0.05}Ni_{0.4}Mn_{0.25}Co_{0.3})O_2/LiPF_6/Li$ cell, we have performed cyclic voltammetry analysis in the potential range between 2 and 5 V at a scan rate of 1 mV s^{-1}. In the current work, the CV analysis is restricted to $Li(Li_{0.05}Ni_{0.4}Mn_{0.25}Co_{0.3})O_2$ owing to the cause that it provides maximum ionic conductivity at ambient temperature among the prepared samples. Figure 8 shows the cyclic voltammogram of fabricated coin cells $Li(Li_{0.05}Ni_{0.4}Mn_{0.25}Co_{0.3})O_2/LiPF_6/Li$. It is quite observed from the voltammogram that lithiation and de-lithiation processes are facetious at the electrode–electrolyte interface. Also, it is observed from the voltammogram that it shows breakdown or abrupt current enhancement during cycling at 3.9, 3.6 V corresponds to lithiation and de-lithiation processes, respectively. This result indicates that the prepared $Li(Li_{0.05}Ni_{0.4}Mn_{0.25}Co_{0.3})O_2$ is electrochemically stable in the operating voltage of battery (2 to 5 V) which is in accordance with earlier reported results by Riley et al. [39]. The weak peaks observed at 4.35, 4.4 V conclude the pair of the $Co^{3+/4+}$ couple [47]. The appearance of peaks at 3.9 and 3.6 V may also be ascribed to the redox couple of $Ni^{2+/4+}$, whereas Mn^{4+} ions are identified as electrochemically inactive which has been reported earlier by Hsieh et al. [48]. The acquired

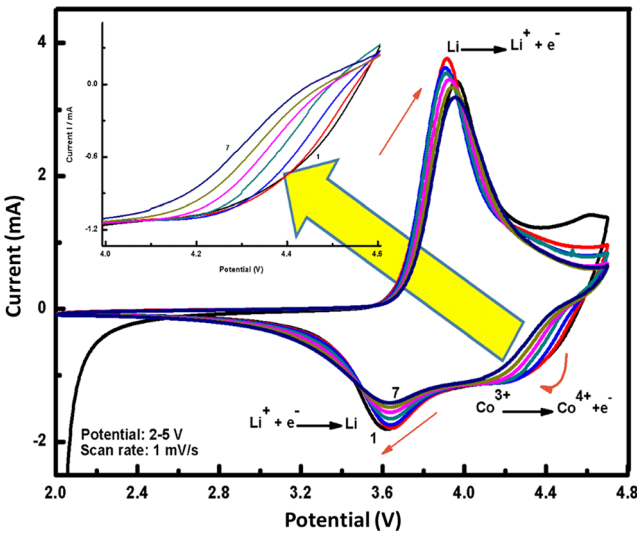

Fig. 8 Cyclic voltammetric curves recorded for $Li(Li_{0.05}Ni_{0.4}Mn_{0.25}Co_{0.3})O_2$ compound with a scan rate of 1 mV s^{-1} for 7 cycles at room temperature

findings are in consistent with the earlier reported results and fit perfectly for battery applications [39].

Galvanostatic battery testing analysis

The charge–discharge curves of the $Li(Li_{0.05}Ni_{0.4}Co_{0.3}Mn_{0.25})O_2/Li$ coin-cell using 1 M LiPF6 are tested by applying current rates (C rates) namely C/2, C, and 2 C, and the results are discussed herein. The Cole–Cole impedance plot of $Li(Li_{0.05}Ni_{0.4}Mn_{0.25}Co_{0.3})O_2$ sample before and after cycling is shown in Fig. 9a. It seems that the resistance of $Li(Li_{0.05}Ni_{0.4}Mn_{0.25}Co_{0.3})O_2$ after cycling process is much smaller than that of the process before cycling. Its corresponding equivalent circuit indicates that it consists of parallel combination of CPE and charge transfer resistance (R_{ct}) connected series to the electrolyte resistance (R_e) before cycling. Where the values of R_e and R_{ct} are 5.488 and 32.843 Ω, respectively. Whereas after cycling, it is observed that it comprises of an addition of parallel combination of resistance and CPE connected series. The three resistance obtained are namely electrolyte resistance R_e, surface layer resistance R_{sl}, and charge transfer resistance R_{ct}, and their corresponding values are 2.628, 10.89, and 16.45 Ω. From this, it is clear that the conductivity of the cell is improved after cycling. Figure 9b shows the charge–discharge characteristics of coin cells fabricated using $Li(Li_{0.05}Ni_{0.4}Mn_{0.25}Co_{0.3})O_2$ powder sample with different current rate values 0.5, 1, and 2 C for 20 cycles in the voltage range between 2.8 and 4.5 V. At the initial stage (first cycle), the value of discharge capacity is found to be in the range of 167, 159, and 123 mAh g^{-1} for three different current rates 0.5, 1, and 2 C. Likewise, the discharge capacity values are found to be 161, 154, and 120 mAh g^{-1} after the 20th cycle. This capacity fade may due to the slow migration of lithium ions while increasing the number of cycles [49]. Figure 9c represents the discharge–capacity as a function of cycles. The capacity fading values has been found in the range between 0.25 and 0.15 mAh g^{-1} at 0.5 and 2 C current rates, respectively.

Its corresponding rate capability curve is plotted which is based on the irreversibile capacity (difference in value between the charge and discharge capacity) and the value of the capacity. The relationship between coulombic efficiency, irreversible capacity, and charge capacity is given in Eq. (5)

$$Q = 1 - \frac{C_{IR}}{C_c} \tag{5}$$

Where Q is the initial coulombic efficiency, C_{IR} is the irreversible capacity, and C_C is the charge capacity [13]. Here, the coulombic efficiency of prepared cathode is about 83–87% for 2, 1, and 0.5 C, respectively. Hence, the prepared layered oxide cathode material paves a way to utilize as an active positive electrode for rechargeable lithium ion batteries.

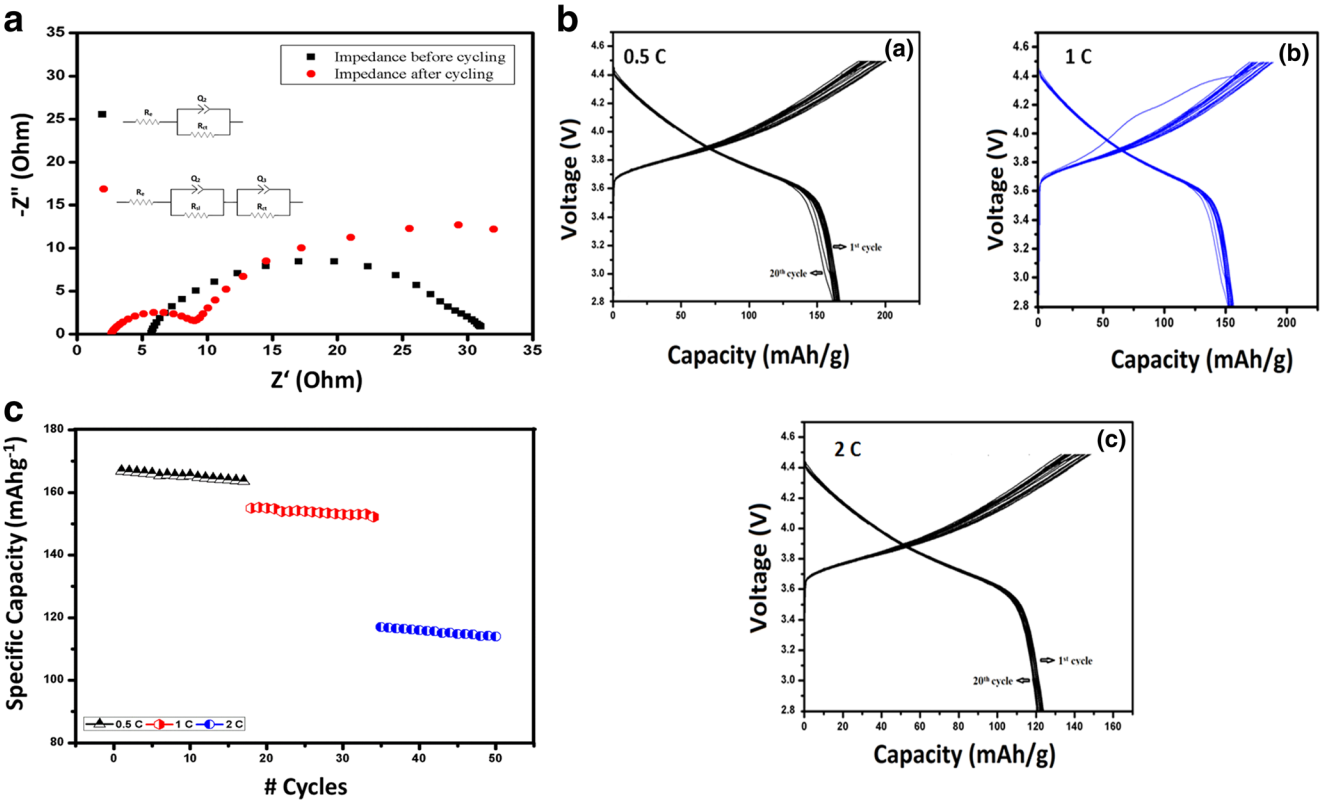

Fig. 9 **a** Electrochemical impedance spectroscopic curves of $Li(Li_{0.05}Ni_{0.4}Mn_{0.25}Co_{0.3})O_2$ compound (a) before 20 cycles and (b) after 20 cycles. **b** Charge–discharge characteristics of $Li(Li_{0.05}Ni_{0.4}Mn_{0.25}Co_{0.3})O_2$ compound obtained with current rate 0.5, 1, and 2 C for 20 cycles. **c** Rate capability curve of $Li(Li_{0.05}Ni_{0.4}Mn_{0.25}Co_{0.3})O_2$

Conclusions

Lithium-rich $Li(Li_{0.05}Ni_{0.7-x}Mn_{0.25}Co_x)O_2$ compound with nanodimension was prepared by using facile sol–gel technique which exhibited hexagonal (α–$NaFeO_2$) structure. The asymmetric M–O stretching mode O–M–O bending mode of $Li(Li_{0.05}Ni_{0.7-x}Mn_{0.25}Co_x)O_2$ were confirmed and in detail investigated through FTIR and Raman spectroscopic analyses. The presence of various elements in the prepared samples and their morphology were investigated by SEM with EDX and HR-TEM analyses. Among the prepared cathode samples, the sample with mole percentage three showed a maximum ionic conductivity at ambient temperature and it was found to be in the range of 10^{-4} S cm^{-1}. The fabricated coin cell provided a maximum discharge capacity of 161 mAh g^{-1} at a current rate of 0.5 C.

Acknowledgements The author thankfully remember the help rendered by Dr. Hirankumar, C-SAR, PSNCET, Tirunelveli, for providing electrochemical workstation for the charge–discharge analysis. The author Dr. KKS gratefully acknowledges the Sophisticated Analytical Instrument Facility (SAIF), IIT Bombay, for providing HR-TEM and FE-SEM facilities and the Dongguk University-Seoul for their financial support.

References

1. Tarascon J-M, Armand M (2001) Issues and challenges facing rechargeable lithium batteries. Nature 414(6861):359–367
2. Chen Z, Dahn J (2002) Effect of a ZrO2 coating on the structure and electrochemistry of Li_xCoO2 when cycled to 4.5 V. Electrochem Solid-State Lett 5(10):A213–A216
3. Wang C-C, Manthiram A (2013) Influence of cationic substitutions on the first charge and reversible capacities of lithium-rich layered oxide cathodes. J Mater Chem A 1(35):10209–10217
4. Gummow R, Liles D, Thackeray M (1993) Spinel versus layered structures for lithium cobalt oxide synthesised at 400 C. Mater Res Bull 28(3):235–246
5. Gummow R, Thackeray M, David W, Hull S (1992) Structure and electrochemistry of lithium cobalt oxide synthesised at 400 C. Mater Res Bull 27(3):327–337
6. Chen H, Qiu X, Zhu W, Hagenmuller P (2002) Synthesis and high rate properties of nanoparticled lithium cobalt oxides as the cathode material for lithium-ion battery. Electrochem Commun 4(6):488–491
7. Nohma T, Kurokawa H, Uehara M, Takahashi M, Nishio K, Saito T (1995) Electrochemical characteristics of $LiNiO_2$ and $LiCoO_2$ as a positive material for lithium secondary batteries. J Power Sources 54(2):522–524
8. Rossouw M, Liles D, Thackeray M (1993) Synthesis and structural characterization of a novel layered lithium manganese oxide, $Li_{0.36}Mn_{0.91}O_2$, and its lithiated derivative, $Li_{1.09}Mn_{0.91}O_2$. J Solid State Chem 104(2):464–466
9. Whittingham MS (2004) Lithium batteries and cathode materials. Chem Rev 104(10):4271–4302

10. Fergus JW (2010) Recent developments in cathode materials for lithium ion batteries. J Power Sources 195(4):939–954
11. Nichelson A, Karthickprabhu S, Karuppasamy K, Hirankumar G, Sahaya Shajan X (2016) A brief review on integrated (layered and spinel) and olivine nanostructured cathode materials for lithium ion battery applications. Mater Focus 5(4):324–334
12. Yu H, Zhou H (2012) Initial coulombic efficiency improvement of the $Li_{1.2}Mn_{0.567}Ni_{0.166}Co_{0.067}$ O_2 lithium-rich material by ruthenium substitution for manganese. J Mater Chem 22(31):15507–15510
13. Koyama Y, Tanaka I, Adachi H, Makimura Y, Ohzuku T (2003) Crystal and electronic structures of superstructural $Li_{1-x}[Co_{1/3}Ni_{1/3}Mn_{1/3}]O_2$ ($0 \leq x \leq 1$). J Power Sources 119:644–648
14. Shi S, Tu J, Tang Y, Liu X, Zhang Y, Wang X, Gu C (2013) Enhanced cycling stability of Li $[Li_{0.2}Mn_{0.54}Ni_{0.13}Co_{0.13}]$ O_2 by surface modification of MgO with melting impregnation method. Electrochim Acta 88:671–679
15. Liu Q, Du K, Guo H, Z-d P, Y-b C, Hu G-r (2013) Structural and electrochemical properties of Co–Mn–Mg multi-doped nickel based cathode materials $LiNi_{0.9}Co_{0.1-x}[Mn_{1/2}Mg_{1/2}]_xO_2$ for secondary lithium ion batteries. Electrochim Acta 90:350–357
16. Cho T, Park S, Yoshio M, Hirai T, Hideshima Y (2005) Effect of synthesis condition on the structural and electrochemical properties of Li $[Ni_{1/3}Mn_{1/3}Co_{1/3}]$ O_2 prepared by carbonate co-precipitation method. J Power Sources 142(1–2):306–312
17. Zheng X, Li X, Zhang B, Wang Z, Guo H, Huang Z, Yan G, Wang D, Xu Y (2016) Enhanced electrochemical performance of $LiNi_{0.8}Co_{0.1}Mn_{0.1}O_2$ cathode materials obtained by atomization co-precipitation method. Ceram Int 42(1):644–649
18. Ying P-Z, Qiu X-Y, Zhang Q-Q, Zhuang Q-C (2015) Synthesis and electrochemical properties of Li-rich cathode material Li $[Ni_xLi_{(1/3-2x/3)}Mn_{(2/3-x/3)}]$ O_2 (x = 1/4, 1/3) for Li-ion battery. Ionics 21(3):657–665
19. Suresh P, Rodrigues S, Shukla A, Vasan H, Munichandraiah N (2005) Synthesis of $LiCo_{1-x}Mn_xO_2$ from a low-temperature route and characterization as cathode materials in Li-ion cells. Solid State Ionics 176(3):281–290
20. Kang S-H, Belharouak I, Sun Y-K, Amine K (2005) Effect of fluorine on the electrochemical properties of layered Li $(Ni_{0.5}Mn_{0.5})O_2$ cathode materials. J Power Sources 146(1):650–653
21. Du C, Zhang F, Ma C, Wu J, Tang Z, Zhang X, Qu D (2015) Synthesis and electrochemical properties of $Li_{1.2}Mn_{0.54}Ni_{0.13}Co_{0.13}O_2$ cathode material for lithium-ion battery. Ionics:1–10
22. Song MY, Mumm DR, Park CK, Park HR (2012) Cycling performance of $LiNi_{1-y}M_yO_2$ (M = Ni, Ga, Al and/or Ti) synthesized by wet milling and solid-state method. Met Mater Int 18(3):465–472
23. Ju S, Koo H, Kim D, Hong S, Kang Y, Ha H, Kim K (2006) Submicron size Li $(Ni_{1/3}Co_{1/3}Mn_{1/3})O_2$ particles prepared by spray pyrolysis from polymeric precursor solution. J Mater Sci Mater Electron 17(5):353–359
24. Park KS, Cho MH, Jin SJ, Nahm KS, Hong Y (2004) Effect of Li ion in transition metal sites on electrochemical behavior of layered lithium manganese oxides solid solutions. Solid State Ionics 171(1):141–146
25. Hwang B, Santhanam R, Liu D (2001) Characterization of nanoparticles of $LiMn_2O_4$ synthesized by citric acid sol–gel method. J Power Sources 97:443–446
26. Kittel C, McEuen P (1976) Introduction to solid state physics, vol 8 Wiley New York
27. Velumani S, Narayandass SK, Mangalaraj D (1998) Structural characterization of hot wall deposited cadmium selenide thin films. Semicond Sci Technol 13(9):1016
28. Laha S, Morán E, Sáez-Puche R, Alario-Franco M, dos Santos-Garcia A, Gonzalo E, Kuhn A, Natarajan S, Gopalakrishnan J, Garcia-Alvarado F (2013) Li_3MRuO_5 (M = Co, Ni), new lithium-rich layered oxides related to $LiCoO_2$: promising electrochemical performance for possible application as cathode materials in lithium ion batteries. J Mater Chem A 1(36):10686–10692
29. Hewston TA, Chamberland B (1987) A survey of first-row ternary oxides $LiMO_2$ (M = Sc-Cu). J Phys Chem Solids 48(2):97–108
30. Song L, Tang Z, Chen Y, Xiao Z, Li L, Zheng H, Li B, Liu Z (2016) Structural analysis of layered Li_2MnO_3–$LiMO_2$ (M = $Ni_{1/3}Mn_{1/3}Co_{1/3}$,$Ni_{1/2}Mn_{1/2}$) cathode materials by Rietveld refinement and first-principles calculations. Ceram Int 42(7):8537–8544
31. Jeong SK, Song C-H, Nahm KS, Stephan AM (2006) Synthesis and electrochemical properties of Li $[Li_{0.07}Ni_{0.1}Co_{0.6}Mn_{0.23}]O_2$ as a possible cathode material for lithium-ion batteries. Electrochim Acta 52(3):885–891
32. Gao Y, Yakovleva M, Ebner W (1998) Novel $LiNi_{1-x}Ti_{x/2}Mg_{x/2}O_2$ compounds as cathode materials for safer lithium-ion batteries. Electrochem Solid-State Lett 1(3):117–119
33. Kim H-S, Kong M, Kim K, Kim I-J, Gu H-B (2007) Effect of carbon coating on $LiNi_{1/3}Mn_{1/3}Co_{1/3}O_2$ cathode material for lithium secondary batteries. J Power Sources 171(2):917–921
34. Valanarasu S, Chandramohan R, Somasundaram R, Srikumar S (2011) Structural and electrochemical properties of Eu-doped $LiCoO_2$. J Mater Sci Mater Electron 22(2):151–157
35. Thanikaikarasan S, Mahalingam T, Sundaram K, Kathalingam A, Kim YD, Kim T (2009) Growth and characterization of electrosynthesized iron selenide thin films. Vacuum 83(7):1066–1072
36. Prince E, Wilson AJC, Hahn T, Shmueli U (1999) International tables for crystallography. International Union of Crystallography,
37. Huang W, Frech R (1996) Vibrational spectroscopic and electrochemical studies of the low and high temperature phases of $LiCo_{1-x}M_xO_2$ (M= Ni or Ti). Solid State Ionics 86:395–400
38. Julien C, Camacho-Lopez M, Mohan T, Chitra S, Kalyani P, Gopukumar S (2000) Combustion synthesis and characterization of substituted lithium cobalt oxides in lithium batteries. Solid State Ionics 135(1):241–248
39. Riley LA, Van Atta S, Cavanagh AS, Yan Y, George SM, Liu P, Dillon AC, Lee S-H (2011) Electrochemical effects of ALD surface modification on combustion synthesized $LiNi_{1/3}Mn_{1/3}$ $Co_{1/3}O_2$ as a layered-cathode material. J Power Sources 196(6):3317–3324
40. Baddour-Hadjean R, Pereira-Ramos J-P (2009) Raman microspectrometry applied to the study of electrode materials for lithium batteries. Chem Rev 110(3):1278–1319
41. Jin X, Xu Q, Yuan X, Zhou L, Xia Y (2013) Synthesis, characterization and electrochemical performance of Li $[Li_{0.2}Mn_{0.54}Ni_{0.13}Co_{0.13}]O_2$ cathode materials for lithium-ion batteries. Electrochim Acta 114:605–610
42. Ghosh P, Mahanty S, Basu RN (2008) Effect of silver addition on the properties of combustion synthesized nanocrystalline $LiCoO_2$. Mater Chem Phys 110(2):406–410
43. Menetrier M, Rougier A, Delmas C (1994) Cobalt segregation in the $LiNi_{1-y}Co_yO_2$ solid solution: a preliminary ^{7}Li NMR study. Solid State Commun 90(7):439–442
44. Marichal C, Hirschinger J, Granger P, Menetrier M, Rougier A, Delmas C (1995) ^{6}Li and ^{7}Li NMR in the $LiNi_{1-y}Co_yO_2$ solid solution (0. ltoreq. y. ltoreq. 1). Inorg Chem 34(7):1773–1778
45. Rao BN, Venkateswarlu M, Satyanarayana N (2014) Electrical and dielectric properties of rare earth oxides coated $LiCoO_2$ particles. Ionics 20(2):175–181
46. Khatun F, Gafur M, Ali M, Islam M, Sarker M (2014) Impact of lithium composition on structural, electronic and optical properties of lithium cobaltite prepared by solid-state reaction. J Sci Res 6(2):217–231
47. Shaju K, Subba Rao G, Chowdari B (2002) Performance of layered Li$(Ni_{1/3}Co_{1/3}Mn_{1/3})O_2$ as cathode for Li-ion batteries. Electrochim Acta 48(2):145–151

48. Hsieh C-T, Mo C-Y, Chen Y-F, Chung Y-J (2013) Chemical-wet synthesis and electrochemistry of $LiNi_{1/3}Co_{1/3}Mn_{1/3}O_2$ cathode materials for Li-ion batteries. Electrochim Acta 106:525–533

49. Spotnitz R (2003) Simulation of capacity fade in lithium-ion batteries. J Power Sources 113(1):72–80